Appl. Phys. B (2015) 119:607–620
DOI 10.1007/s00340-015-6077-1

Applied Physics B
Lasers and Optics

# Effect of recondensation of sublimed species on nanoparticle temperature evolution in time-resolved laser-induced incandescence

**F. Memarian[1] · F. Liu[1] · K. A. Thomson[1] · K. J. Daun[2] · D. R. Snelling[1] · G. J. Smallwood[1]**

Received: 9 October 2014 / Accepted: 7 March 2015 / Published online: 27 March 2015


**Abstract** In high-fluence laser-induced incandescence (LII), current LII models significantly overpredict the soot nanoparticle temperature decay rate compared to that inferred from two-color pyrometry at the first 100 ns after the peak laser pulse in atmospheric pressure flames. One possible cause is the back flow of sublimed species, which to date has been neglected in LII modeling. In this study, the transient direct simulation Monte Carlo (DSMC) method has been used, for the first time, to calculate the temperature evolution of soot particles, taking into account recondensation of sublimed species. In this algorithm, the physical time is discretized into a number of time steps called ensemble time steps, and the heat flux is calculated by performing several DSMC runs in each ensemble time step before proceeding to the next ensemble time step until the variance reaches an acceptable value. This heat flux is then used to update the nanoparticle temperature over the ensemble time step. Using the new algorithm, the temperature evolution of the particle can be predicted by the DSMC code, which is an improvement to previous DSMC simulations in which predetermined temperature decay curves must be prescribed. The results show that recondensation of sublimed species on the originating nanoparticle is not significant. Although accounting for condensation of sublimed species originating from neighboring soot particles enhances the role of recondensation of sublimed species in slowing down the soot particle temperature decay, it is still not sufficient to be considered as a plausible cause for the discrepancy between modeled soot temperature and the two-color pyrometry measured one in high-fluence LII.

✉ F. Liu
Fengshan.liu@nrc-cnrc.gc.ca

[1] MSS, National Research Council Canada, 1200 Montreal Rd, Ottawa, ON K1A 0R6, Canada

[2] Department of Mechanical and Mechatronics Engineering, University of Waterloo, 200 University Avenue West, Waterloo, ON N2L 3G1, Canada

## List of symbols

| | |
|---|---|
| $a$ | Particle radius (nm) |
| $c_o$ | Speed of light in vacuum, $2.998 \times 10^8$ (m s$^{-1}$) |
| $c_p$ | Specific heat [J/(kg K)] |
| $D_{eq}$ | Equivalent diameter of soot aggregate (nm) |
| $d_p$ | Primary particle diameter (nm) |
| $f_a$ | Equivalent sphere scaling prefactor |
| $h$ | Planck's constant, $6.626 \times 10^{-34}$ (J s) |
| $I_\lambda$ | Spectral radiation intensity (W/m$^2$ μm sr) |
| $J_\lambda$ | Spectral incandescence intensity (W/m$^2$ μm sr) |
| $k_B$ | Boltzmann's constant, $1.38 \times 10^{-23}$ [J/(molecule K)] |
| $M$ | Mass of soot particle (kg) |
| $M_v$ | Average molecular weight of sublimed clusters (kg/mol) |
| $N_p$ | Number of primary particles in an aggregate |
| $P(a)$ | Probability density function of particle size |
| $P_g$ | Gas pressure (Pa) |
| $P_v$ | Partial pressure of sublimed species (Pa) |
| $q_{abs}$ | Laser absorption rate (W) |
| $Q_{abs,\lambda}$ | Spectral absorption efficiency |
| $q_{conc}$ | Conduction heat transfer rate (W) |
| $q_{evap}$ | Evaporation heat transfer rate (W) |
| $q_{rad}$ | Radiation heat transfer rate (W) |
| $R$ | Universal gas constant (J/mol K) |
| $t$ | Time (s) |
| $T_g$ | Gas temperature (K) |
| $T_p$ | Particle temperature (K) |
| $U$ | Average velocity of sublimed clusters (m/s) |
| $\alpha$ | Thermal accommodation coefficient |

| | |
|---|---|
| $\beta$ | Sublimation/condensation coefficient |
| $\varepsilon_a$ | Equivalent sphere scaling exponent |
| $\lambda$ | Wavelength ($\mu$m) |
| $\rho_s$ | Soot density (kg/m$^3$) |

**Subscripts and superscripts**

| | |
|---|---|
| G | Gas |
| P | *P*article |

## 1 Introduction

Laser-induced incandescence (LII) is a widely used technique for inferring the volume fraction and primary particle size distribution of aerosolized nanoparticles, including combustion-generated particulate matter in laminar and turbulent diffusion flames [1] and engine exhaust [2]. In this technique, a high-power laser pulse of nanoseconds duration heats the suspended nanoparticles to incandescence temperatures. After the laser pulse, the nanoparticles cool by heat transfer to the surrounding gas, during which time the spectral incandescence signal is measured. Soot volume fraction has been shown to be proportional to the LII signal in the visible wavelength region; hence, the calibrated signal may be used to infer this quantity [3]. Moreover, since the temperature decay depends on the primary particle size, in principle the nanoparticle size distribution can be inferred from the time-resolved incandescence data provided that the heat transfer rate is modeled accurately. The total heat transfer rate is the superposition of the contribution of different mechanisms that include sublimation, conduction, radiation, absorption, oxidation and annealing [4–7].

Based on the magnitude of the excitation laser fluence, LII experiments can be divided into low-fluence and high-fluence LII. In low-fluence LII, sublimation is negligible, and since radiation is not significant at atmospheric pressure [8–10], the temporal evolution of the nanoparticle temperature is determined by a balance between conduction and laser energy absorption.

Sublimation occurs when the laser heats the soot nanoparticles to approximately 3800–4000 K [4, 11, 12] which is close to the sublimation temperature of pure graphite, such LII experiments are called high-fluence LII. Sublimation persists in the cooling phase as long as the nanoparticle temperature remains close to the sublimation temperature. In high-fluence LII, sublimation dominates other cooling mechanisms, and hence, the nanoparticle temperature is determined by an energy balance between sublimation and laser energy absorption during the laser pulse.

Significant research has been devoted to modeling heat conduction from laser-energized nanoparticles. Melton [13] was the first to propose a model for the evolution of nanoparticle temperature, size and incandescence. He modeled heat conduction using the continuum heat transfer equations and accounted for rarefaction effects using a correction factor. Following his work, there have been several efforts to develop heat conduction models in the transition regime for monomers [14] and aggregates [15–17], and, most recently, to determine the thermal accommodation coefficient using molecular dynamics [18]. The thermal accommodation coefficient defines the average energy transfer during molecular scattering and is used to calculate heat conduction in the free-molecular and transition regimes.

The state of the art of sublimation modeling is comparatively immature; the discrepancy between experimental results and LII model predictions in high laser fluences [1, 19–21] is often attributed to inaccurate sublimation models. In particular, Smallwood et al. [20] addressed some of the weaknesses of the Melton model. First, they retained the use of a sublimation coefficient, $\beta$, following the work of Hofeldt [22], in determining the mass flux of sublimation; this coefficient is originally introduced for calculating the condensation rate to account for the fact that not all incident species will condense on the surface, and more details could be found in Ref. [23]. Second, they noticed a mistake in the molecular weight that had been used by Melton in association with the heat of sublimation. The sublimed vapor is comprised of several species, and the heat of sublimation is the energy required to sublime one mole of solid material into several carbonaceous species; hence, the mean molecular weight of sublimed species needs to be used, whereas in Melton's model, the atomic weight of carbon had been used instead. They also corrected the expression for calculating the mass flux of vapor and the thermal conductivity of air.

The modern LII models discussed above do not fully consider the gas dynamics of sublimed species. In the sublimation models listed in Ref. [20] and more recent work [6, 21], the Clausius–Clapeyron equation has been used to calculate the equilibrium value of partial pressure of carbon clusters based on the nanoparticle temperature, which has in turn been used to calculate the unilateral sublimation rate from kinetic theory equations. The term unilateral is used to refer to sublimation leaving a surface as opposed to the net sublimation, which is the difference between the unilateral sublimation and condensation. The implicit assumption in these models is that sublimation occurs in the free-molecular regime, but the equilibrium rate of unilateral sublimation can still be used, and the gas dynamics of the sublimed species does not play an important role in nanoparticle cooling.

There is little knowledge about the gas dynamics of sublimation and whether neglecting gas dynamics effects of sublimed species could partially account for the discrepancy between the LII model and experiments. In particular, it has been hypothesized that some of the sublimed species

may recondense on the surface of the soot particles, which may reduce the heat transfer rate due to sublimation [1]. These recondensing clusters may originate from the same soot particle where they originate, or come from neighboring soot particles.

In a previous study [24], the transient direct simulation Monte Carlo (DSMC) method has been used for the first time to simulate sublimation from a single soot nanoparticle using a predetermined temperature decay curve to investigate the possibility of the back flux of sublimed species and the formation of shock waves. Contrary to some speculation in the literature [7], these simulations did not reveal the formation of strong shocks under conditions typical of LII, but showed that some of the sublimed clusters return back to the subliming particle surface as a result of intermolecular collisions with the surrounding gas and other sublimed clusters. In the simplified model used in that study, the incident sublimed clusters were simply reflected from the particle surface back into the flow field and the direct effect of sublimation and recondensation on heat transfer was not considered. It was further shown that the sublimed cloud acts as a "snowplow" and pushes away the inert gas molecules and hence decreases the number flux of their incidence on the surface which consequently affects the rate of heat conduction.

In the current study, the energy balance equation is incorporated into the transient DSMC simulation and is used to update the nanoparticle temperature at predefined time steps. Such calculation requires a low-variance estimate of the heat transfer rate over each time step, which is achieved using a novel ensemble averaging technique. The transient DSMC code is used to simulate nanoparticle temperature decay under conditions that represent typical high-fluence LII experiments conducted in a laminar sooting diffusion flame at atmospheric pressure. A single soot aggregate is considered using a one-dimensional computational domain of spherical shape. From the beginning of the laser pulse, the energy balance of the aggregate is performed in the DSMC code to update the soot temperature. Two different boundary conditions of the sublimed species ($C_3$ in this study) at the outer boundary of the DSMC solution domain were considered, namely "vacuum" and "specularly reflecting." The implications of each choice are described. At the soot aggregate surface, the sublimation rate is determined by the instantaneous soot temperature, and then, the interactions between the sublimed species and between the sublimed species and the surrounding gas molecules are modeled in the transient DSMC. Analysis of the results shows that regardless of the boundary condition at the outer solution domain boundary, the recondensation of sublimed species does not make significant contribution to affect soot particle temperature evolution.

## 2 Laser-induced incandescence

In time-resolved LII (TiRe-LII), the incandescence signal of laser-energized particles is in general measured in the cooling phase when heat transfer to the surrounding gas starts to dominate laser energy absorption. At any instant, the total LII signal is due to the combined incandescence from all nanoparticle size classes in the detection volume according to

$$J_\lambda(t) = C_\lambda \int_0^\infty \pi a^2 P(a) Q_{\mathrm{abs},\lambda}(a) I_{b,\lambda}[T_\mathrm{p}(t,a)]\mathrm{d}a \tag{1}$$

where $P(a)$ is the size distribution of soot primary particles, $Q_{\mathrm{abs},\lambda}$ is the absorption efficiency, $C_\lambda$ is a calibration constant, which depends on the particle loading and the detector optics, $T_\mathrm{p}(t,a)$ is the instantaneous temperature of the particles, and $I_{\mathrm{b},\lambda}$ is the blackbody intensity at $T_\mathrm{p}$,

$$I_{\mathrm{b},\lambda}(T_\mathrm{p}) = \frac{2hc_\mathrm{o}^2}{\lambda^5}\left[\exp\left(\frac{hc_\mathrm{o}}{\lambda k_\mathrm{B} T_\mathrm{p}}\right) - 1\right]^{-1} \tag{2}$$

In principle, the size distribution of the nanoparticles, $P(a)$, can be found from the LII signal decay. This is often done by assuming that $P(a)$ obeys a prescribed type of distribution (e.g., lognormal) and then carrying out nonlinear regression of modeled spectral incandescence data or pyrometrically derived effective temperatures to experimental measurements [25].

To generate modeled data, temperatures for a range of nanoparticle size classes are substituted into Eq. (1), and then, the integration is performed. The temperature curves are found by solving the energy balance equation

$$\rho_\mathrm{s} c_\mathrm{p} \frac{4\pi a^3}{3}\frac{\mathrm{d}T_\mathrm{p}}{\mathrm{d}t} = q_\mathrm{abs}(t,a) - q_\mathrm{cond}(t,a) - q_\mathrm{rad}(t,a) - q_\mathrm{evap}(t,a) \tag{3}$$

At atmospheric or higher pressures, radiation heat transfer is negligible [3, 4, 6, 8]; hence, conduction and evaporation are the only significant cooling mechanisms. In high-fluence LII, evaporation is dominant during and shortly after the laser pulse [4, 5, 20].

At temperatures above the sublimation threshold, gaseous carbon clusters ranging from $C_1$ to $C_{10}$ are sublimed from the particle surface based on thermodynamic considerations, see [5] and the references cited therein. Assuming that the unilateral rate of sublimation is not affected by the actual partial vapor pressure near the surface, the equilibrium relationship can be used for calculating this quantity; hence, the rate at which sublimation occurs can be calculated from [20],

$$\left(\frac{\mathrm{d}M}{\mathrm{d}t}\right)_\mathrm{evap} = \frac{1}{2}\rho_\mathrm{s}\pi d_\mathrm{p}^2 \frac{\mathrm{d}}{\mathrm{d}t}(d_\mathrm{p}) = -\pi d_\mathrm{p}^2 \beta P_\upsilon U \tag{4}$$

where $d_p$ is the soot particle diameter, $U$ is the average velocity of the sublimed clusters as they depart from the surface and is derived from the Maxwellian velocity distribution at the soot temperature $T_p$, and $P_v$ in Eq. (4) is the equilibrium value of vapor pressure of the sublimed species, which is found from the Clausius–Clapeyron equation,

$$P_v = P^* \exp\left(\frac{\Delta H_{sub}(T_p - T^*)}{RT_pT^*}\right) \quad (5)$$

where $P^*$ and $T^*$ are the reference pressure and temperature and $\Delta H_{sub}$ is the enthalpy of formation of sublimed carbon species [26]. It should be noted that the Clausius–Clapeyron equation is based on the assumption of phase equilibrium, even though the sublimation process during LII is highly non-equilibrium. Leider et al. [27] have used the Clausius–Clapeyron equation to produce data for vapor pressure, and a fifth-order polynomial fit to that data as presented in [20] has been used to calculate the vapor pressure at each temperature.

To understand why $\beta$, which is the sublimation/condensation coefficient, is introduced in Eq. (4), one should note that the kinetic theory cannot directly predict the rate of unilateral sublimation because it is a surface phenomenon, but the rate of unilateral condensation can be predicted by the kinetic theory. Under equilibrium conditions, however, the rate of unilateral condensation and sublimation are equal; hence, the same relationship can be used for the rate of unilateral sublimation. In order to drive Eq. (4), it has been assumed that the subliming particle is surrounded by an equilibrium cloud of sublimed species and the rate of incidence of molecules on the surface is calculated using the kinetic theory [23]. Since not all the incident molecules condense on the surface, a coefficient smaller than unity must be applied to the rate of incidence to predict the correct rate of unilateral condensation; such a coefficient is called the condensation/sublimation coefficient, $\beta$, which is a function of surface and sublimed species properties. The average velocity of sublimed molecules in Eq. (4) is calculated from

$$U = \sqrt{\frac{M_v}{2\pi RT_p}} \quad (6)$$

where $M_v$ is the mean molecular weight of sublimed species and $R$ is the universal gas constant [20]. It should be noted that with this definition of $\beta$, Eq. (4) does not account for the recondensation of sublimed species. If this equation is to be used in an LII model as the net rate of evaporation, another coefficient needs to be introduced to account for recondensation.

Despite the recent enhancements to LII modeling [6], there still exist many sources of uncertainty in modeling sublimation: (1) the sublimation/condensation coefficient is not well defined for soot; (2) the enthalpy and entropy of sublimation of carbon clusters from soot are not available in the literature, since these parameters vary considerably depending on fuel chemistry and the flame conditions, so the properties of bulk graphite are usually used instead; (3) changes in the microstructure of soot, such as annealing of the soot surface, can affect sublimation rate; (4) the effect of aggregate shielding in the presence of sublimation is not known; (5) nonthermal photo-desorption during the laser pulse may contribute to sublimation/evaporation [5, 6] but is not considered in this study; and (6) gas dynamics of sublimation may affect particle cooling but it has not been quantitatively studied yet.

One of the speculated gas dynamics effects, which has been neglected in LII models but can potentially affect the cooling of particles, is the recondensation of evaporated species [1]. The focus of this paper is to investigate the importance of recondensation of sublimed carbon species using the transient version of DSMC method.

## 3 Transient direct simulation Monte Carlo method (DSMC)

Bird's original unsteady DSMC code [28] is the basis for the current code used in this study to model transient sublimation and condensation during LII.

Figure 1 shows the schematic of the computational domain used in this study, which is a spherically symmetric 1D geometry. Like control volume CFD simulations, the computational domain needs to be discretized into a

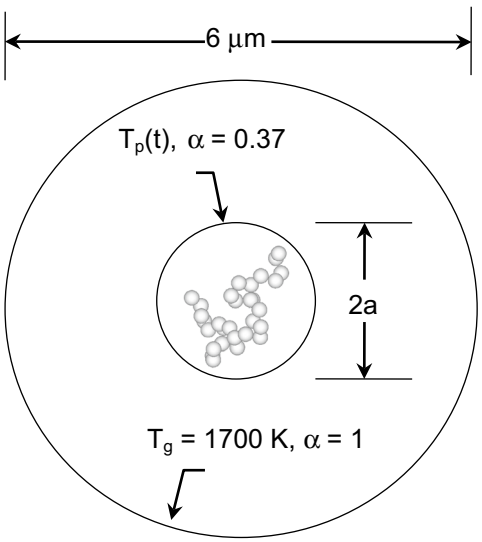


**Fig. 1** A schematic of the DSMC simulation geometry (not to scale). The parameters indicated in the figure are used in most of the DSMC calculations in this study

number of computational volumes called cells. The purpose of using cells is to limit the choice of collision partners to molecules within a cell and also to accumulate statistical information to be used in calculating macroscopic properties. Due to the spherical symmetry of the problem, the discretization is needed only along the radial direction from the inner boundary (particle surface) to an outer boundary. To discretize the computational domain, 150 equally spaced cells in the radial direction have been used. The cell size is a computational parameter that needs to be chosen considering the gradients in the gas, i.e., it should be small enough to be able to capture the gradients. If the cell size is too large, the gradients will be underpredicted. As a general rule, the cell size needs to be smaller than 1/3 of the local mean free path [28].

In contrast to the steady state DSMC, in which time averaging is used to reduce the variance in macroscopic properties predicted by the simulation, in the transient DSMC, ensemble averaging is used for this purpose. To calculate surface phenomena such as the heat transfer rate, however, both ensemble and time averaging are used in transient DSMC. To perform ensemble averaging, a number of independent simulations are carried out using different initial conditions that all correspond to the same macroscopic state, but are microscopically different due to the use of different random seeds. The samples taken from each simulation are then used to calculate the macroscopic properties and surface fluxes.

The purpose of this paper is to investigate the effect of gas dynamics on heat transfer rate from nanoparticles and consequently on their temperature. Bird's original method of ensemble averaging cannot be used for this purpose, since it requires the nanoparticle temperature to be predefined at each time step, and thus cannot capture the nonlinear interaction between the gas dynamics that governs heat transfer from the nanoparticle, and the nanoparticle cooling curve. In the new ensemble averaging technique, an "ensemble time step" has been defined as the time period over which the temperature of the particle is updated. The ensemble time step is chosen to be similar to that used in LII modeling, i.e., it is small enough to resolve the rapid soot temperature variation within the laser pulse but large enough to span many DSMC time steps to increase the sample size. The inner and outer boundary conditions are known at the beginning of the simulation, and the initial state of the gas inside the computational domain is produced using an equilibrium distribution at the temperature and pressure of the outer boundary (ambient values). A predetermined number of independent simulations are carried out, based on numerical experiments discussed below, all starting at time zero over the duration of an ensemble time step. During this time, the nanoparticle temperature is assumed to be constant. For each of these simulations, the state of the flow field (velocity, position and other relevant information of each molecule) is stored at the end of the ensemble time step to be used as the initial condition for the corresponding simulation of the next ensemble time step. Once all the simulations during the first ensemble time step have been performed, ensemble averaging as well as time averaging (over the ensemble time step) is carried out to calculate a single value for the conduction and sublimation heat transfer rate at the end of the first ensemble time step in the main DSMC code, other terms of the heat transfer equation are averaged over the ensemble time step in the same manner as for the LII model, and finally, the particle temperature is updated using Eq. (3). This updated particle temperature is used as the boundary condition on the inner surface for the next ensemble time step. The next series of simulations are performed for the second ensemble time step, starting at the end of the first time step and this marching in time continues until the last ensemble time step. In the simulations performed in this study, the total simulation time is 100 ns and is divided into 100 equal ensemble time steps, so each ensemble time step is 1 ns. Each run adds to the sample size, and the reduction in statistical error is related to the square root of the sample size [29, 30].

It should be noted that the variance in heat transfer rate and consequently on the particle temperature is reduced as the number of runs performed in each ensemble time period increases, but the simulation time is directly proportional to the number of runs; hence, the number of runs has been optimized to satisfy both a low enough variance in the results and a reasonable computational time. Based on these criteria, the simulation has been performed using 200 runs which lead to a maximum relative standard deviation of $1.5 \times 10^{-4}$ for the sublimation heat transfer rate. Figure 2 shows a logarithmic plot of the relative standard deviation of the mean versus the number of simulations for sublimation heat transfer rate at a certain ensemble time step, which corresponds to 20 ns from the beginning of the laser pulse. As this figure shows, the slope of the logarithmic curve is $-0.5$, which is because the relative standard deviation of the mean decreases in proportion to the inverse square root of the sample size and the sample size is proportional to the number of runs.

The computational time for each simulation with $10^6$ simulated molecules and 200 runs is about 48-h clock time on a single 3.40 GHz CPU computer.

Since soot exists as aggregates rather than isolated primary particles, it is necessary to account for aggregation in the simulation. Transient 3D DSMC simulations for an aggregate structure in detail are not computationally tractable; instead, an equivalent sphere, with diameter $D_{eq}$, given by the relationship below [31] has been used

$$D_{eq} = d_p \left(N_p / f_a\right)^{(1/2\varepsilon_a)} \tag{7}$$

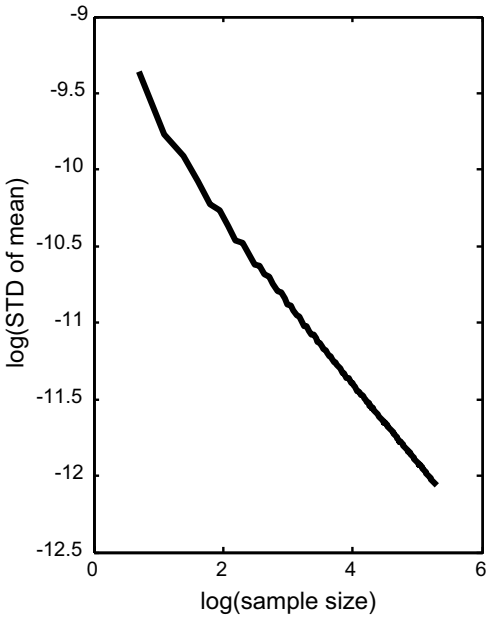


**Fig. 2** The logarithm (base 10) of the relative standard deviation of the mean versus logarithm of the sample size for the sublimation heat transfer rate at 20 ns after the onset of the laser pulse

where $d_p$ is the mean diameter of primary particles, which is 29.7 nm at 42 mm above the burner exit on the centerline of a laminar coflow ethylene diffusion flame based on TEM image analysis [32], and $N_p$ is the number of primary particles in the aggregate. The equivalent sphere scaling prefactor, $f_a$, and scaling exponent, $\varepsilon_a$, are given as

$$f_a = 1.04476 + 0.22329\alpha + 7.14286 \times 10^{-3}\alpha^2 \quad (8)$$

and

$$2\varepsilon_a = 1.99345 + 0.30224\alpha - 0.11276\alpha^2 \quad (9)$$

based on steady DSMC calculations conducted in the free-molecular regime [16]. The gas molecule is assumed to scatter from the nanoparticle surface according to the Maxwell scattering kernel with $\alpha = 0.37$, which is in accordance with other DSMC studies performed for conduction heat transfer in the transition regime [14, 33]. It should be pointed out that most of the physical conditions selected in the present unsteady DSMC calculations are based on those in [1]. It is also noticed that the scaling prefactor and exponent are dependent on the thermal accommodation coefficient. The physical significance of such dependence has been discussed by Filippov et al. [15]. The equivalent sphere obtained using this relationship accounts for the shielding effect in the case of pure conduction, but is unable to consider the complex interaction of sublimed species that are trapped in the structure of the aggregate. It is understood that using an equivalent sphere to represent the detailed aggregate structure can cause uncertainties in molecular transport (conduction and sublimation) since it neglects intermolecular collisions within the aggregate structure, but there is no better alternative currently to deal with this issue given the unaffordability of performing 3D transient DSMC calculations. In addition, the main concern in this paper is to compare DSMC and LII model predictions, so using a consistent equivalent sphere size in the two methods serves this purpose.

The surface of the equivalent sphere forms the inner boundary of the computational domain. The outer boundary is chosen such that its radius is half of the average distance between adjacent aggregates, which can be estimated based on the soot volume fraction at the location under consideration, e.g., for a soot volume fraction of 4 ppm, and aggregates consisting of an average of 28 primary particles of size 29.7 nm, and the average distance between adjacent aggregates is about six microns [1]. In this study, we have considered larger aggregates but still used the same computational domain size. It should be noted that the simulation is not sensitive to the domain size as long as the effect of neighboring aggregates is not taken into account. The physical implication of this choice is that the sublimed species and any other perturbation reaching the outer boundary will arrive at the same times as sublimed species and perturbations from neighboring aggregates. Since the soot vapor is mainly composed of $C_3$ in the temperature ranges typical to LII [27], $C_3$ is assumed to be the only sublimed carbon cluster for simplicity.

Air molecules reaching the outer boundary are removed from the flow field, but new air molecules are allowed to enter based on the assumed pressure and temperature at the location of the boundary. Since we do not know how the pressure and temperature of the gas change with time at the location of the outer boundary, they are approximated to remain constant at the initial atmospheric values. This assumption is expected to be reasonable in this study since the calculations are only performed up to 100 ns, and the outer boundary temperature and pressure should not be altered significantly due to heat and mass transfer from the nanoparticle in this time frame.

For carbon clusters, the interaction of $C_3$ with the outer boundary has been modeled using two different boundary conditions. In the "vacuum boundary condition," any $C_3$ molecule that reaches the boundary is removed from the simulation. The vacuum boundary condition is equivalent to assuming that no $C_3$ molecules exist outside the solution domain, which is a good approximation at short time intervals when few carbon species have reached the boundary, but does not account for any influx of carbon clusters sublimed from neighboring aggregates into the solution domain.

To better represent what happens at the outer boundary, we need to allow the sublimed carbon clusters to re-enter

the DSMC solution domain, which accounts for the entering of sublimed carbon clusters from the neighboring aggregates. To do this, we need to know the number flux and velocity characteristics of the $C_3$ clusters that need to be introduced into the flow field. For the purpose of introducing a proper boundary condition at the outer boundary, we need to analyze the total volume of gas heated by the laser beam first. It is reasonable to treat this volume as a closed system at short times because the diffusion speed is not large enough to let significant amount of mass transfer across the boundaries [1]. Consider $N_{agg}$ aggregates in this volume which are distributed evenly on a Cartesian grid; also assume that the total number of evaporated clusters at each moment is $N_{C3}$. If the total volume is divided to $N_{agg}$ smaller control volumes of equal size which are drawn over the centers of aggregates, then at each moment, there are $N_{C3}/N_{agg}$ evaporated species at each control volume (due to the equal contribution of all the aggregates). Also further assume that the state of the flow field at every control volumes is identical (which is true if the total area heated by the laser is much larger than individual control volumes around the aggregates, except for those close to the edge of the laser beam).

The boundary condition for an isolated aggregate needs to ensure the existence of the correct number of molecules in that control volume at each moment to be consistent with the mass balance at the larger scale. This can be achieved by introducing a new $C_3$ cluster to replace each $C_3$ cluster leaving the local control volume, or, as is done in this study, a specularly reflecting boundary condition can be used at the outer boundary of the DSMC computational domain for $C_3$ clusters. Specular reflection reserves all the characteristics of molecules except for their radial velocity, which is reversed. If the control volumes were cubes with faces located halfway between neighboring aggregates, this treatment would be very accurate, because the characteristics of entering $C_3$ molecules would be similar to those exiting the flow field due to the general symmetry of the problem. In this study, a spherical boundary has been used instead of a cubic boundary and this treatment is still a reasonable simplification as long as the mean free path is significantly smaller than the radius of curvature of the outer domain. For LII experiments under flame temperature (~1700 K), the overall mean free path is about 600 nm [33], which is about one-fifth the radius of curvature. While this method will achieve an appropriate conservation of $C_3$ cluster mass in the region heated by the laser beam, it is not certain that the kinetic energy imparted to the incoming $C_3$ clusters via a specular reflection is strictly correct and it may lead to an overprediction of the recondensation effect. Nevertheless, this is a simple model to account for the gas dynamic interactions between subliming neighboring aggregates.

The time step in DSMC calculations needs to meet two criteria: First, it needs to be smaller than the mean collision time, and second, it must be small enough so that molecules do not travel a distance larger than the cell size in a single time step. Based on these criteria, a DSMC time step of $10^{-11}$ s was found suitable for this study. In contrast to steady state DSMC, in which the time step carries no physical meaning and can be adjusted for numerical convenience, in transient DSMC, the passage of each time step is equivalent to the passage of physical time. The ballistic motion of molecules during each time step is completely deterministic and occurs at the latest velocity stored for each molecule; this velocity only changes when the molecule undergoes collision with another molecule or the boundaries. In contrast to the deterministic motion of molecules, the collision process is stochastic. The probability that two molecules within a cell collide with each other is proportional to their relative velocity and their collision cross section [28].

In DSMC, instead of modeling each real molecule individually, a number of them are represented by a single molecule called the simulated molecule [28]. The number of real molecules represented by each simulated molecule is a computational parameter that needs to be predefined in each simulation. In this study, this ratio has been set to 500 to ensure the existence of at least 25 simulated molecules at each cell. The outer boundary radius is 3 μm, which corresponds to the LII experiments in a Gülder burner laminar ethylene/air coannular diffusion flame at a measurement height of 42 mm above the burner exit surface, where the mean separation distance of soot aggregates is about 6 μm [1]. The initial number of real air molecules in the solution domain is about $5 \times 10^8$; hence, there are initially about $10^6$ simulated molecules in the solution domain.

To model the interaction of species in DSMC, collisional properties need to be specified for each species. The intermolecular collision model used in this study is the variable soft sphere (VSS) model developed by Bird [28]. The ambient gas is air with a viscosity temperature index of 0.58 and reciprocal of the VSS scattering parameter of 0.73 [28]. Air is assumed to be composed of a single molecule with specific collisional properties as listed in [28]. Corresponding information for $C_3$ is not available in the literature; however, the collisional properties of carbon dioxide, which is structurally similar to $C_3$ (both are linear triatomic and have a similar molecular mass), have been used instead. The number of internal degrees of freedom considered for $C_3$ and air is two in the temperature range of interest. Since the rotational degrees of freedom are excited in the simulations performed in this study, the VSS scattering law alone will not be able to model the energy transfer that occurs at intermolecular collisions. Therefore, the Larsen–Borgnakke collision model [34] has been used for

this purpose. In this model, the total energy of the collision pair remains intact after the collision but is redistributed between the internal and translational modes so that the energy in each mode conforms to its equilibrium distribution. To implement this method, the collisions are sampled as either elastic or inelastic and relaxation collision number determines the ratio of elastic collisions to the total number of collisions [28, 34]. Although the rotational relaxation rate changes with temperature, due to the unavailability of a general temperature relationship, a constant value of five has been used in this study based on the recommendation made in [28]. A sensitivity analysis showed the results are insensitive to this parameter. In the elastic collisions, a simple VSS scattering law is employed to determine the post-collision properties of the colliding pair, while for the inelastic collisions, the Larsen–Borgnakke model is used first to redistribute energy between modes, and then, the VSS scattering law is called to calculate the translational velocity of each molecule.

In the case of a gas mixture in which collisions may occur between different species, the diameters, masses, number of degrees of freedom and temperature exponents for the coefficient of viscosity, $\omega_{12}$, may be different for the two colliding molecules. To deal with this situation, the average of the two exponents for the coefficient of viscosity is used. The same approach is used for the rotational degrees of freedom, $\zeta_{12}$ [28]. When there is a collision between similar molecules, however, the parameters for homogeneous collision are used.

It should be noted that, each time two $C_3$ molecules collide, there is a possibility for sticking and forming a larger cluster; however, this effect is neglected in this study since nucleation of new particles is not expected to occur significantly at short times after the laser pulse. Instead, collision between $C_3$ molecules has been treated as a non-sticking event in which the two molecules are scattered after the collision based on the VSS collision model.

Finally, it should be pointed out that the diameter of the equivalent sphere representing the soot aggregate is assumed constant during the transient DSMC calculations to avoid the complexities of dealing with a moving inner boundary at the particle surface. To be consistent with the assumptions made in the DSMC calculations, the equivalent sphere diameter and mass are also kept constant in the calculations of the LII model. This assumption affects the particle temperature evolution, but the purpose of the paper is to compare the particle temperature evolution predicted by the transient DSMC method to the LII model of Liu et al. [4], so it is a valid assumption as long as the drop in mass or diameter of the aggregate is not significant. In the case of flame temperature (1700 K) with a laser fluence of 1.8 mJ/mm$^2$ at 1064 nm, if the aggregate is assumed as an equivalent sphere, the LII model of Liu et al. [4] shows a drop of 11 % in mass due to sublimation at the first 100 ns after the beginning of the laser pulse, corresponding to a drop in aggregate diameter of about 3.8 %, which is considered insignificant.

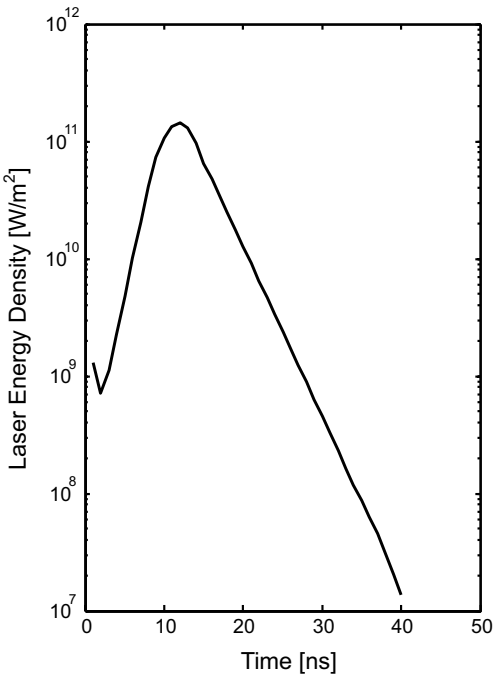


**Fig. 3** The temporal laser energy density profile for a laser fluence of 1.8 mJ/mm$^2$

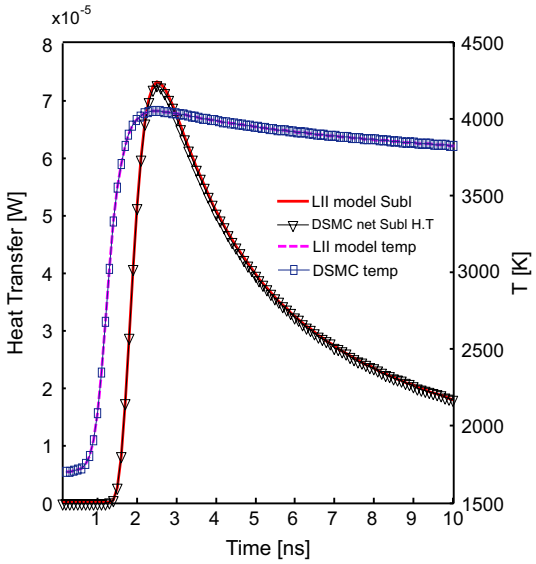


**Fig. 4** Comparison of DSMC and LII results for the net sublimation heat transfer rate for the vacuum boundary condition. Calculations are conducted for evaporation coefficient = 0.3, an equivalent sphere diameter of 182 nm, the initial gas temperature = 1700 K and the laser fluence = 1.35 mJ/mm$^2$

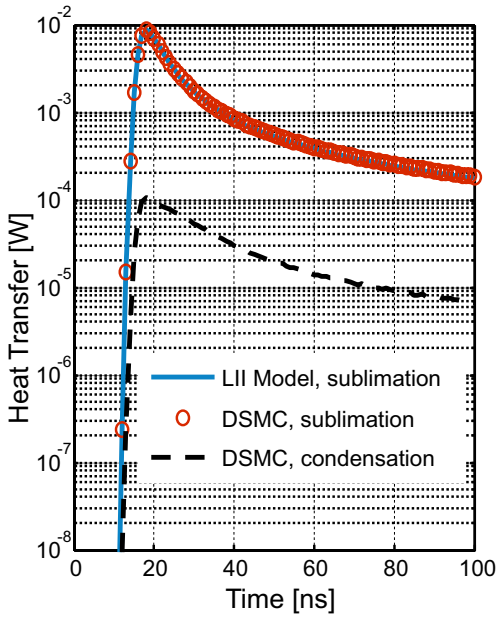


**Fig. 5** The effect of recondensation on the sublimation heat transfer rates: vacuum boundary condition, $\beta = 1$

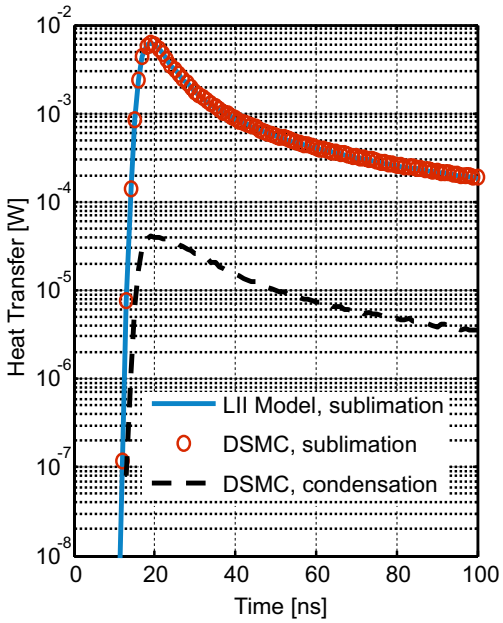


**Fig. 6** The effect of recondensation on the sublimation heat transfer rates: vacuum boundary condition, $\beta = 0.5$

## 4 Results and discussion

In this study, the laser wavelength is 1064 nm. Figure 3 shows the temporal laser profile used in this study, which corresponds to a laser fluence of 1.8 mJ/mm$^2$. It is noticed that the laser energy density is plotted in the log scale. This temporal laser profile is the same as that considered in previous studies, e.g., [31, 33]. When plotted in the linear scale, e.g., in [31, 33], it is easier to observe that the total laser duration is about 27 ns (corresponding to the moment when the laser energy density drops to below 1 % of the peak) and the FWHM duration is about 7 ns. In order to validate the DSMC code, the heat transfer rate and temperature predicted by DSMC and LII are compared for a specific case in Fig. 4. This figure corresponds to the first 100 ns after the beginning of the laser pulse. Since the LII model neglects the recondensation of sublimed species, the effect of recondensation is also neglected in this particular DSMC simulation to provide equal conditions for a direct comparison. As can be seen, there is near-perfect agreement between the two model's prediction of temperature and heat transfer rate. This comparison serves as validation for the new DSMC simulation developed in this study.

Figures 5 and 6 compare the effect of recondensation on the heat transfer rate for sublimation/condensation coefficients of 1 and 0.5, respectively. In both cases, the laser fluence is 1.8 mJ/mm$^2$. The soot aggregate is composed of 200 primary particles, corresponding to an equivalent sphere diameter of 353 nm following Eq. (7), and the vacuum boundary condition has been used for $C_3$. In the

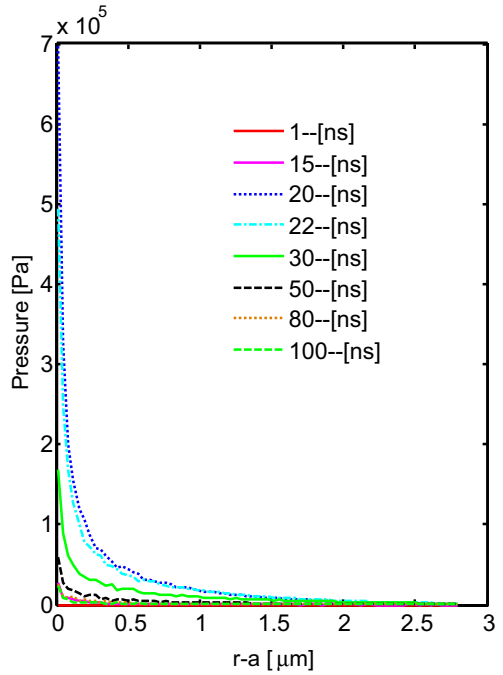


**Fig. 7** The evolution of the partial pressure of $C_3$ at different moments after the onset of the laser pulse

case of Fig. 6, the implication of the sublimation/condensation coefficient of 0.5 is that only half of the incident species will recondense on the surface of the soot aggregate, whereas in Fig. 5, where $\beta = 1$, all the incident species will condense on the surface. In regard to the rate of

sublimation, the rate is twice as large for $\beta = 1$ compared to $\beta = 0.5$ for each temperature. A larger $\beta$ means a higher rate of sublimation but also a higher rate of recondensation. The comparison between Figs. 5 and 6 shows that the net sublimation rate increases by increasing $\beta$.

Unless otherwise explicitly indicated, the following conditions were used hereafter in all the calculations: laser fluence 1.8 mJ/mm$^2$, an equivalent sphere diameter of 353 nm, $T_g = 1700$ K, $\beta = 1$.

To gain a better understanding of the physics of sublimation, it is useful to analyze the change in the partial pressure profiles of $C_3$ and air during the laser pulse. Figures 7 and 8 show the time evolution of the partial pressure profiles of $C_3$ and air, respectively, after the onset of the laser pulse under the same conditions as Fig. 5. The number density evolution of $C_3$ and the bath gas have been discussed in a previous work [24], where a predetermined temperature decay curve was used. As can be observed from Fig. 7, the partial pressure of $C_3$ near the nanoparticle surface first increases rapidly after the onset of the laser pulse to reach a peak at about 20–22 ns, where the soot temperature peaks as shown in Fig. 4, and then decreases at longer times. Correspondingly, the particle pressure of air close to the particle surface first decreases rapidly to reach a minimum at 20 ns and then recovers toward the ambient pressure. However, the rapid increase in the partial pressure of $C_3$ near the particle surface due to sublimation alone cannot cause a significant amount of recondensation. If the sublimed cloud of $C_3$ were in phase equilibrium, the condensation rate would be the same as the sublimation rate, but the short time scales typical of LII preclude phase equilibrium. Phase equilibrium could only be approached when sublimation occurs at a steady state in an enclosed space for a sufficiently long time. In this case, however, as can be observed from Fig. 9, the sublimed cloud has a large bulk velocity in the positive radial direction (away from the nanoparticle) and that is one reason why the ratio of condensation to sublimation is so low. In Fig. 9, the increase in velocity near the outer boundary for each curve is a consequence of the particular boundary condition used for $C_3$, which assumes vacuum of $C_3$ outside the outer boundary.

Another reason why the ratio of condensation to sublimation is small is the spherical expansion of the sublimed species. In order to show how geometry can affect the rate of back flow and consequently the recondensation rate, it is useful to compare spherical and planar geometry results. Several researchers have studied pulsed laser ablation of material into vacuum or in the presence of a background gas in the planar geometry [35–39]. To understand the effect of geometry, a DSMC simulation has been performed for a planar one-dimensional geometry with the computational domain being the area between two infinite surfaces, the inner surface is located at one equivalent sphere radius to the right of the coordinate origin, and the outer surface is at 3 μm away from the origin. The boundary conditions are similar to the spherical case except the way the temperature of the inner boundary is treated. Since the energy balance equation cannot be used on the inner surface in case of planar geometry, the particle temperature profile

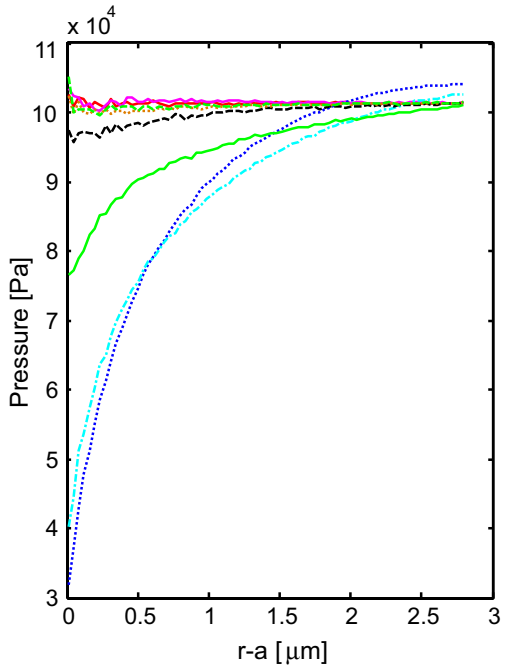


**Fig. 8** The evolution of the partial pressure of air at different moments after the onset of the laser pulse

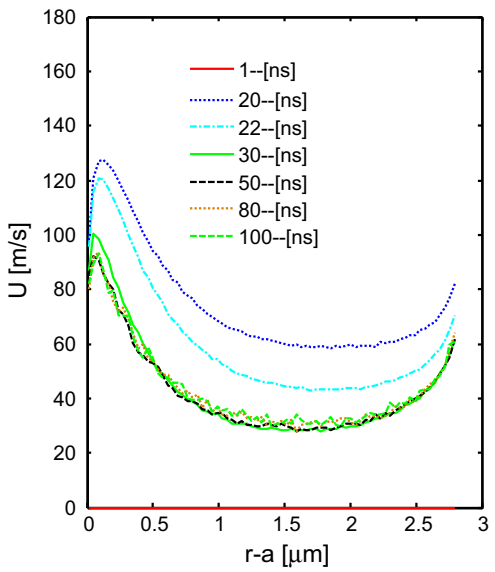


**Fig. 9** Evolution of the bulk radial velocity of the sublimed $C_3$ molecules at different times after the onset of the laser pulse

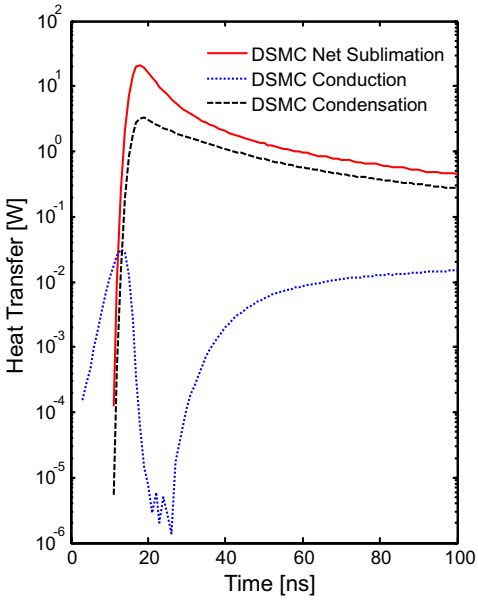


**Fig. 10** Heat transfer rates of DSMC in the planar geometry

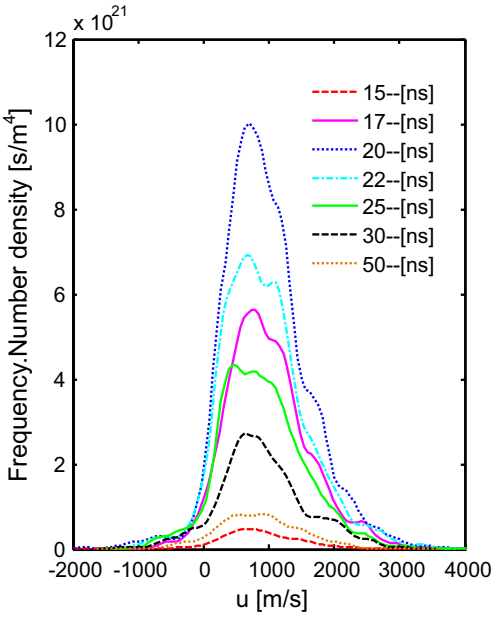


**Fig. 11** The radial velocity distribution of $C_3$ at cell 1 located 10 nm away from the particle surface at different times after the onset of the laser pulse

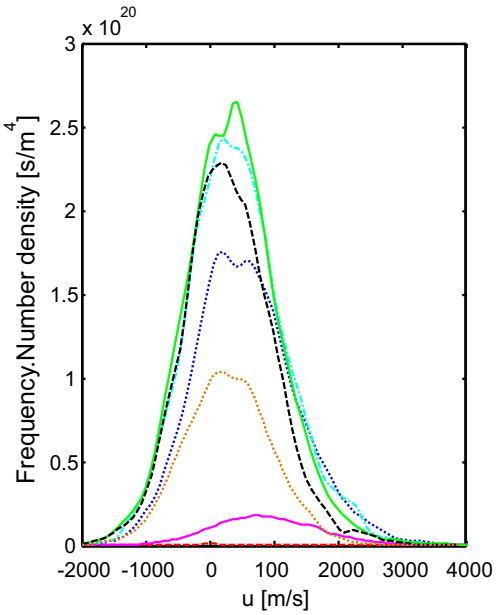


**Fig. 12** The velocity distribution of $C_3$ at cell 75 located 1.4 μm away from the particle surface at different times after the onset of the laser pulse

obtained from the corresponding spherical case has been used instead. As is evident in Fig. 10, which corresponds to this planar geometry, the relative importance of the back flux of sublimed species is significantly higher compared to that in the spherical computational domain. Also, the pressure and number density curves for the planar geometry (not shown) indicate that the sublimed species propagate mainly by diffusion and no shock wave is observed. This is in accordance with a previous study [24], but contradicts some of the speculations in the literature [7] about the formation of shock waves in LII.

To further investigate the physics of sublimation and condensation in LII, the velocity distribution of $C_3$ molecules has been plotted at different times (up to 50 ns) at 10 nm away from particle surface, which corresponds to the first cell (the closest one to the particle surface), in Fig. 11. Figure 11 reveals that the distribution is almost half Maxwellian, i.e., the velocity is predominately in the forward direction, at all times as the sublimation is still occurring. This means that the ratio of molecules with negative velocity to those with positive velocity is small, which corresponds to a small condensation rate compared to the sublimation rate. It is useful to compare the velocity distribution at 1.4 μm from the particle surface (which corresponds to the midpoint between the inner and outer boundaries) shown in Fig. 12 to the velocity distribution at 10 nm (Fig. 11). At 1.4 μm, the velocity distribution of $C_3$ molecules is nearly full Maxwellian, because $C_3$ molecules undergo several collisions with air molecules or with other $C_3$ molecules before arriving at this location.

Based on the results presented above, it can be concluded that the rate of recondensation of sublimed clusters on the aggregate from which they have originated is negligible; hence, recondensation of sublimed clusters is not a plausible cause for the discrepancy between the modeled

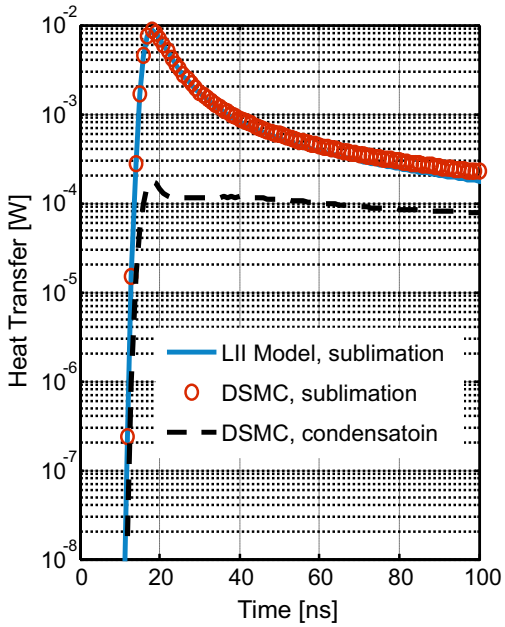


**Fig. 13** Effect of recondensation on sublimation heat transfer rate when using the specularly reflecting boundary condition

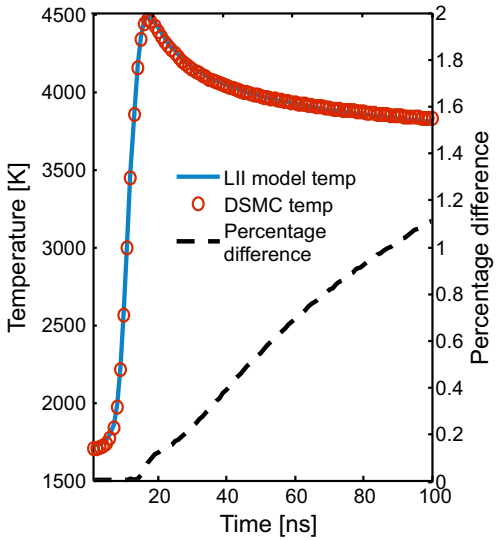


**Fig. 14** Comparison of DSMC and LII temperature evolutions when using the specularly reflecting boundary condition

and measured soot temperature evolutions in high-fluence LII and neglect of recondensation of sublimed species in LII modeling is justified based on the present transient DSMC results. Figures 5 and 6 show that the heat transfer curves predicted by DSMC and LII model are almost identical in this case. However, it should be noted that this finding is based on the "vacuum boundary condition" which does not account for the contributions of the sublimed clusters originating from neighboring soot aggregates.

Figure 13 corresponds to a case where the specularly reflective surface has been used as the outer boundary condition, while the rest of the parameters are the same as those of Fig. 6. The justification for the use of this boundary condition is that in the larger scale, the sublimed clusters will mostly stay in the region excited by the laser beam at short times and will homogeneously fill the volume after a short time. Figure 13 shows that the back flux is more significant compared to the vacuum boundary condition case.

Figure 14 compares the nanoparticle temperature evolution predicted by DSMC and the LII model in the case of the reflecting outer boundary condition. The figure shows that the temperatures predicted by DSMC are slightly higher than the LII model after the peak of the laser pulse and the difference increases with time; this is due to the more pronounced condensation rate predicted by using the specularly reflecting boundary condition, which reduces the net heat transfer rate. The temperature difference predicted by the two methods increases with time and reaches a value of roughly one percent at 100 ns. However, such a difference is still too small to render recondensation as a plausible cause for the discrepancy between the modeled and measured soot temperatures in high-fluence LII.

## 5 Conclusions

This paper examines the effect of recondensation of sublimed carbon species on the temperature evolution of soot particle in the early stage of high-fluence LII. While previous research has used steady state and transient DSMC to study the gas dynamics surrounding the nanoparticle in LII experiments, this is the first time that the transient DSMC has been used to predict soot temperature evolution during high-fluence LII where the particle temperature is updated using the surface heat transfer rates from the DSMC calculations. Two different types of boundary condition have been applied for the outer boundary of the computational domain. The vacuum boundary condition neglects any effect of the sublimed carbon clusters from the neighboring aggregates, and the condensation rate predicted using this type of boundary condition is negligible. This implies that the percentage of sublimed species that returns to the aggregate from which they originate is negligible.

The specularly reflecting surface boundary condition was introduced to semi-quantitatively account for the sublimed carbon clusters from the neighboring aggregates entering the solution domain. Use of this boundary condition shows an enhanced rate of recondensation. The increased condensation rate slows down the soot particle temperature decay rate slightly, but is not significant enough to render recondensation as a plausible cause for the discrepancy

between the modeled and measured soot temperatures in high-fluence LII. The present DSMC results suggest that recondensation of sublimed carbon clusters is negligible and can be safely neglected in LII modeling. Further research is required to explore other mechanisms responsible for the discrepancy between the modeled and measured soot temperatures in high-fluence LII.

In future work, we will apply the model for a wider range of ambient pressures, gas temperatures, particle sizes and soot volume fractions to investigate their effect on the significance of recondensation. The model will also be modified to be used for simulating the gas dynamics in the larger area heated by the laser beam.

## References


1. D.R. Snelling, K.A. Thomson, F. Liu, G.J. Smallwood, Comparison of LII derived soot temperature measurements with LII model predictions for soot in a laminar diffusion flame. Appl. Phys. B **96**, 657–669 (2009)
2. S. Schraml, S. Will, A. Leipertz, Simultaneous measurement of soot mass concentration and primary particle size in the exhaust of a DI diesel engine by time-resolved laser-induced incandescence (TIRE-LII). SAE Technical Paper 1999-01-0146
3. H. Bladh, P.E. Bengtsson, Characteristics of laser-induced incandescence from soot in studies of a time-dependent heat-and mass-transfer model. Appl. Phys. B **78**, 241–248 (2004)
4. F. Liu, B.J. Stagg, D.R. Snelling, G.J. Smallwood, Effects of primary soot particle size distribution on the temperature of soot particles heated by a nanosecond pulsed laser in an atmospheric laminar diffusion flame. Int. J. Heat Mass Transf. **49**, 777–788 (2006)
5. H.A. Michelsen, Understanding and predicting the temporal response of laser-induced incandescence from carbonaceous particles. J. Chem. Phys. **118**, 7012–7045 (2003)
6. H.A. Michelsen, F. Liu, B.F. Kock et al., Modeling laser-induced incandescence of soot: a summary and comparison of LII models. Appl. Phys. B **87**, 503–521 (2007)
7. H.A. Michelsen, P.O. Witze, D. Kayes, S. Hochgreb, Time-resolved laser-induced incandescence of soot: the influence of experimental factors and microphysical mechanisms. Appl. Opt. **42**, 5577–5590 (2003)
8. C.J. Dasch, Continuous-wave probe laser investigation of laser vaporization of small soot particles in a flame. Appl. Opt. **23**, 2209–2215 (1984)
9. D.R. Snelling, G.J. Smallwood, I.G. Campbell, J.E. Medlock, Ö.L. Gülder, Development and application of laser-induced incandescence by comparison with extinction measurements in laminar premixed, flat flames. Proceedings of AGARD 90th Symposium of the Propulsion and Energetics Panel on Advanced Non-intrusive Instrumentation for Propulsion Engines, Brussels, Belgium (1997)
10. S. Will, S. Schraml, K. Bader, A. Leipertz, Performance characteristics of soot primary particle size measurements by time-resolved laser-induced incandescence. Appl. Opt. **37**, 5647–5658 (1998)
11. N.E. Olofsson, J. Johnsson, H. Bladh, P.E. Bengtsson, Soot sublimation studies in a premixed flat flame using laser-induced incandescence (LII) and elastic light scattering (ELS). Appl. Phys. B **112**, 333–342 (2013)
12. F. Goulay, L. Nemes, P.E. Schrader, H.A. Michelsen, Spontaneous emission from C2(d 3Πg) and C3(A 1Πu) during laser irradiation of soot particles. Mol. Phys. **108**, 1013–1025 (2010)
13. L.A. Melton, Soot diagnostics based on laser heating. Appl. Opt. **23**, 2201–2208 (1984)
14. A. Filippov, D.E. Rosner, Energy transfer between an aerosol particle and gas at high temperature ratios in the Knudsen transition regime. Int. J. Heat Mass Transfer **43**, 127–138 (2000)
15. A.V. Filippov, M. Zurita, D.E. Rosner, Fractal-like aggregates: relation between morphology and physics properties. J. Colloid Interface Sci. **229**, 261–273 (2000)
16. F. Liu, M. Yang, F.A. Hill, D.R. Snelling, G.J. Smallwood, Influence of polydisperse distributions of both primary particle and aggregate size on soot temperature in low-fluence LII. Appl. Phys. B **83**, 383–395 (2006)
17. J. Johnsson, H. Bladh, N.E. Olofsson, P.E. Bengtsson, Influence of soot aggregate structure on particle sizing using laser-induced incandescence: importance of bridging between primary particles. Appl. Phys. B **112**, 321–332 (2013)
18. K.J. Daun, G.J. Smallwood, F. Liu, Molecular dynamics simulations of translational thermal accommodation coefficients for time-resolved LII. Appl. Phys. B **94**, 39–49 (2009)
19. S. Schraml, S. Dankers, K. Bader, S. Will, A. Leipertz, Soot temperature measurements and implications for time-resolved laser-induced incandescence. Combust. Flame **120**, 439–450 (2000)
20. G.J. Smallwood, D.R. Snelling, F. Liu, Ö.L. Gülder, Clouds over soot evaporation: errors in modeling laser-induced incandescence. ASME J. Heat Transf. **123**, 814–818 (2001)
21. C. Schulz, B.F. Kock, M. Hofmann, H. Michelsen, S. Will, B. Bougie, R. Suntz, G. Smallwood, Laser-induced incandescence: recent trends and current questions. Appl. Phys. B **83**, 333–354 (2006)
22. D.L. Hofeldt, Real-time soot concentration measurement technique for engine exhaust streams. Society of Automotive Engineers, SAE Paper No. 930079
23. E.H. Kennard, *Kinetic Theory of Gases* (McGraw-Hill, New York, 1938)
24. F. Memarian, K.J. Daun, Gas dynamics of sublimed nanoclusters in high fluence time-resolved laser-induced incandescence. Numer. Heat Transf. Part B Fundam. **65**, 393–409 (2014)
25. K.J. Daun, B.J. Stagg, F. Liu, G.J. Smallwood, D.R. Snelling, Determining aerosol particle size distributions using time-resolved laser-induced incandescence. Appl. Phys. B **87**, 363–372 (2007)
26. A.C. Eckbreth, Effects of laser-modulated particulate incandescence on Raman scattering diagnostics. J. Appl. Phys. **48**, 4473–4479 (1977)
27. H.R. Leider, O.H. Krikorian, D.A. Young, Thermodynamic properties of carbon up to the critical poit. Carbon **11**, 555–563 (1973)
28. G.A. Bird, *Molecular Gas Dynamics and the Direct Simulation of Gas Flows* (Clarendon Press, Oxford, 1994)
29. M.A. Fallavollita, D. Baganoff, J.D. McDonald, Reduction of simulation cost and error for particle simulations of rarefied flows. J. Comput. Phys. **109**, 30–36 (1993)
30. N.G. Hadjiconstantinou, A.L. Garcia, M.Z. Bazant, G. He, Statistical error in particle simulations of hydrodynamic phenomena. J. Comput. Phys. **187**, 274–297 (2003)
31. D.R. Snelling, F. Liu, G.J. Smallwood, Ö.L. Gülder, Determination of the soot absorption function and thermal accommodation coefficient using low-fluence LII in a laminar coflow ethylene diffusion flame. Combust. Flame **136**, 180–190 (2004)
32. K. Tian, F. Liu, K.A. Thomson, D.R. Snelling, G.J. Smallwood, D. Wang, Distribution of the number of primary particles of soot aggregates in a nonpremixed laminar flame. Combust. Flame **138**, 195–198 (2004)

33. F. Liu, K.J. Daun, D.R. Snelling, G.J. Smallwood, Heat conduction from a spherical nano-particle: status of modeling heat conduction in laser-induced incandescence. Appl. Phys. B **83**, 355–382 (2006)
34. C. Borgnakke, P.S. Larsen, Statistical collision model for Monte Carlo simulation of polyatomic gas mixture. J. Comput. Phys. **18**, 405–420 (1975)
35. C.J. Knight, Theoretical modeling of rapid surface vaporization with back pressure. AIAA J. **17**, 519–523 (1979)
36. T.E. Itina, W. Marine, M. Autric, Nonstationary effects in pulsed laser ablation. J. Appl. Phys. **85**, 7905–7908 (1999)
37. F. Garrelie, J. Aubreton, A. Catherinot, Monte Carlo simulation of the laser-induced plasma plume expansion under vacuum: comparison with experiments. J. Appl. Phys. **83**, 5075–5082 (1998)
38. D. Slbold, H.M. Urbasse, Kinetic study of pulsed desorption flows into vacuum. Phys. Rev. A **43**, 6722–6734 (1991)
39. A.V. Gusarov, I. Smurov, Thermal model of nanosecond pulsed laser ablation: analysis of energy and mass transfer. J. Appl. Phys. **97**, 014307 (2005)